Journal of chemical & engineering data

Article

pubs.acs.org/jced

Mass Diffusion Coefficient and Soret Coefficient of *o*-Dichlorobenzene Solutions of PCBM and [60]Fullerene by the Soret Forced Rayleigh Scattering Method

Hiroaki Matsuura, Shintaro Iwaasa, and Yuji Nagasaka*

Department of System Design Engineering, Keio University, 3-14-1, Hiyoshi, Yokohama 223-8522, Japan

ABSTRACT: We measured the binary diffusion coefficient and the Soret coefficient in the fabrication system of organic photovoltaics (OPVs) by the holographic grating technique we call Soret forced Rayleigh scattering (SFRS). To test the validity of the apparatus we built, we here performed measurements on binary benchmark mixtures: three types of binary solutions (50 wt %) composed of *n*-dodecane, isobutylbenzene, and 1,2,3,4-tetrahydronaphthalene, at 298.2 K. Our experimental results for the diffusion coefficient and the Soret coefficient agree with the benchmark values within ± 10 %. The uncertainties estimated based on the Guide to the Expression of Uncertainty in Measurement (GUM) for the Soret coefficient on the benchmark mixtures are within 16 % with the coverage factor of $k = 2$. For OPV systems, our measurements were performed on [60]fullerene or [6,6]-phenyl-C61-butyric acid methyl ester (PCBM) solved in *o*-dichlorobenzene. We evaluated the Soret coefficient and the diffusion coefficient across a wide concentration range ([60]fullerene/*o*-dichlorobenzene; (5 to 30) mg·mL^{-1} and PCBM/*o*-dichlorobenzene; (10 to 40) mg·mL^{-1}) at 298.2 K and the temperature range (288.2 to 333.2) K.

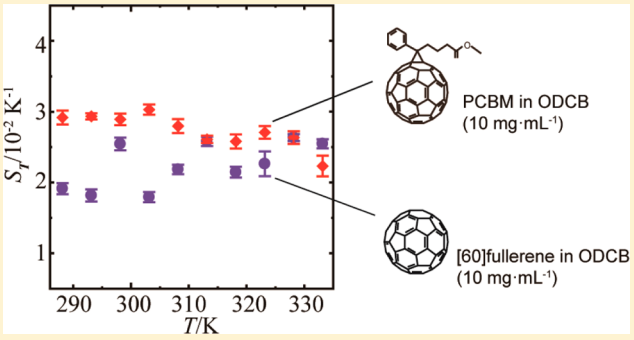

INTRODUCTION

The Soret effect (also called thermal diffusion or thermodiffusion) is a mass transport phenomenon driven by the temperature gradient, whereas mass diffusion is driven by the concentration gradient. In micro- and nanoscale systems, because even a small difference of concentration or temperature induces a considerably large concentration gradient or temperature gradient, the Soret effect and mass diffusion play crucial roles. Progress in this research area relies on the availability of high-quality mass transport property data. The fabrication process of organic photovoltaics (OPVs) is an example of such micro- and nanoscale systems. OPVs have attracted substantial interest as next-generation solar cells because of their promising properties including flexibleness, lightness, and inexpensiveness.[1−3] It is expected that active layers in OPV devices can be fabricated by a wet coating process that leads to large-area and low-cost roll-to-roll production.[4,5]

In a wet coating process, a solvent is volatilized from the surface of a coated solution containing organic semiconductors, and the concentration gradient is formed in a cast liquid film with micrometer- to nanometer-order thickness. Mass diffusion thus significantly affects the quality of the film. Similarly, the temperature gradient formed in the drying process induces the Soret effect. The Soret coefficient as well as the mass diffusion coefficient are thus considered to be important to the optimization of the fabrication process of OPVs. Notably, diffusive mass transport has significant effects on the active-layer morphology, which is related to the performance of OPVs.[6−8] For improvement in the power conversion efficiency, it is necessary to control the nanoscale spatial arrangement.[9−12] As stated above, quantitative evaluations of mass transport phenomena are essential for the development of OPVs, but the available data on the Soret coefficients and diffusion coefficients in OPV fabrication processes are very limited.

Although there have been a few experimental studies on diffusion in polymers such as [6,6]-phenyl-C61-butyric acid methyl ester (PCBM) in poly(3-hexylthiophene-2,5-diyl) (P3HT)[13,14] or [60]fullerene in polyfluorene,[15] the diffusion coefficient and Soret coefficient in cast solution systems have not yet been reported, probably due to the lack of suitable measurement methods. For example, the thermogravitational column (TGC) method,[16] which is one of the typical techniques used to observe the Soret effect, needs a long time for measurement (over 1 h), and the TGC method cannot be used to evaluate the diffusion coefficient and Soret coefficient simultaneously. The optical sensing technique called the beam deflection method[17] may not be suitable for concentrated and deep-colored OPV cast solutions because it has an optical path the length of which is centimeter-order, and a probing laser may be nearly absorbed in the samples. Considering that a universally accepted theoretical model of the Soret effect does not exist,[18] experimental evaluations by other methods are required.

Special Issue: Memorial Issue in Honor of Anthony R. H. Goodwin

Received: July 17, 2015
Accepted: November 4, 2015
Published: November 16, 2015

DOI: 10.1021/acs.jced.5b00609
J. Chem. Eng. Data 2015, 60, 3621−3630

We performed the measurements on OPV systems by the holographic grating technique, which has also been called thermal-diffusion forced Rayleigh scattering (TDFRS) or Soret forced Rayleigh scattering (SFRS). In the early works based on this technique, Thyagarajan and Lallemand observed the mass transport in the binary mixtures (CS_2 and ethanol) and determined the thermodiffusion factor α_T (the product of Soret coefficient and the temperature) in 1978.[19] Köhler and his coworkers later improved the TDFRS technique[20−22] as the simultaneous measurement method for the diffusion coefficient, the thermodiffusion coefficient, and the Soret coefficient, and they employed this technique for the study of the Soret effect in various systems including liquid mixtures[23] and polymer solutions.[24,25] In our laboratory, we constructed the SFRS apparatus for the measurement of the diffusion coefficient in binary mixtures,[26−29] applying the forced Rayleigh scattering (FRS) technique to determine the thermal diffusivity in liquids.[30] In the present study, we reconstructed our SFRS apparatus for the measurement of the Soret coefficient.

To test the validity of the constructed apparatus, we measured binary mixtures which have several measurement examples: the mixtures of toluene/*n*-hexane[17,23,31,32] and the Fontainebleau benchmark mixtures.[33−38] We evaluated the uncertainties based on the Guide to the Expression of Uncertainty in Measurement (GUM). We then measured the diffusion coefficient and Soret coefficient of cast solution systems of OPV (PCBM/*o*-dichlorobenzene and [60]fullerene/*o*-dichlorobenzene) in the temperature range of (288.2 to 333.2) K and the concentration range of (5 to 30) mg·mL^{-1} for [60]fullerene/*o*-dichlorobenzene and (10 to 40) mg·mL^{-1} for PCBM/*o*-dichlorobenzene.

PRINCIPLE OF MEASUREMENT FOR SORET COEFFICIENT

The principle of SFRS for the measurement of diffusion coefficients is described in detail in our previous paper.[29] With the heating laser, the sinusoidal temperature distribution corresponding to the interference fringe is formed in the sample, and this induces the mass transport by the Soret effect. Because the distributions of temperature and concentration form a sinusoidal refractive index distribution, the probing laser irradiating the heating area is diffracted. The mass transport phenomena can be evaluated by the analysis of the diffracted light intensity. A typical example of the output voltage $V(t)$ which is proportional to the light intensity at the detector is shown in Figure 1. The sharp intensity change after the start of the heating indicates the formation of the temperature distribution corresponding to the interference fringe. The relatively slow change after the formation of the temperature distribution indicates the formation of the concentration distribution by the Soret effect. The sharp descent after the end of the heating indicates the decay of the temperature distribution. The gradual descent after the decay of the temperature distribution indicates the decay of the concentration distribution.

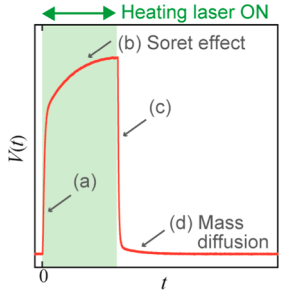

Figure 1. Output signal $V(t)$ of Soret forced Rayleigh scattering (SFRS). (a) Formation of the temperature distribution; (b) formation of the concentration distribution by the Soret effect; (c) decay of the temperature distribution; (d) decay of the concentration distribution by mass diffusion.

The SFRS method has several advantages for the measurement of Soret coefficients and diffusion coefficients in OPV systems. First, the time needed for the measurement is exceedingly short (millisecond-order) compared to the conventional methods (over 10 min or 1 h) because of its micrometer-scale excitation and observation area. Second, SFRS needs only a very small sample volume (within 200 μL), and it is thus useful for the measurements of precious samples. Third, noncontact and *in situ* measurements can be conducted. Moreover, the optical path is so short (within 500 μm) that it is applicable for concentrated and deep-colored samples.

For the measurement of the Soret coefficient, the intensity change of the diffracted light during heating (Figure 1b) as well as that after the heating (Figure 1d) are analyzed, while only the latter was evaluated in our previous study of the diffusion coefficient.[29] In the SFRS model, the concentration in the laser-heated area is described by the following one-dimensional diffusion equation in an *x*-coordinate:[29]

$$\frac{\partial c(x,t)}{\partial t} = D_{12}\frac{\partial^2 c(x,t)}{\partial x^2} + D_T c(x,t)\{1 - c(x,t)\}\frac{\partial^2 T(x,t)}{\partial x^2} \quad (1)$$

in which t is the time and $c(x,t)$ is the mass fraction of the solute. D_{12} is the diffusion coefficient and D_T is the thermal diffusion coefficient. By solving eq 1, the amplitude of the sinusoidal concentration distribution $\Delta c(t)$ is calculated. With this $\Delta c(t)$, the amplitude of refractive index $\Delta n(t)$ is described as

$$\Delta n(t) = \Delta T(t)\left.\frac{\partial n}{\partial T}\right|_{c_0,p_0} + \Delta c(t)\left.\frac{\partial n}{\partial c}\right|_{T_0,p_0} \quad (2)$$

where $\Delta T(t)$ is the amplitude of the sinusoidal temperature distribution calculated from the heat conduction equation,[29] and $\partial n/\partial T$ and $\partial n/\partial c$ are so-called contrast factors related to the dependence of the refractive index on the temperature and the concentration, respectively. T_0 and p_0 are the measuring temperature and pressure, respectively, and c_0 is the initial concentration of the sample. The diffraction efficiency for the Bragg condition is in proportion to the squares of the amplitude of the refractive index $\Delta n(t)$.[39] By eq 2, the intensity of the diffracted light $I_1(t)$ for a sufficient amount of time after the formation of the temperature distribution is expressed as follows:

$$I_1(t) \propto \left[\frac{\partial n}{\partial T} - S_T c_0(1 - c_0)\left\{1 - \exp\left(-\frac{t}{\tau_D}\right)\right\}\frac{\partial n}{\partial c}\right]^2 \quad (3)$$

$S_T = D_T/D_{12}$ is the Soret coefficient, and τ_D is the decay time constant of the concentration, described by

$$\tau_D = \frac{1}{D_{12}}\left(\frac{\Lambda}{2\pi}\right)^2 \quad (4)$$

DOI: 10.1021/acs.jced.5b00609
J. Chem. Eng. Data 2015, 60, 3621−3630

where Λ is the fringe spacing. Similarly, $I_1(t)$ during the heating for a sufficient amount of time after the formation of the temperature distribution is expressed as follows:[29]

$$I_1(t) \propto \exp\left(-\frac{t}{\tau_D}\right)^2 \quad (5)$$

In the analysis of the detected signal, the effect of the coherent and incoherent scattered light superimposed over the diffracted light is considered. The output voltage $V(t)$, which is proportional the light intensity at the detector, is described as[39]

$$V(t) \propto I_1^2 + 2\sqrt{I_1 I_c}\cos\psi + I_c + I_{inc} \quad (6)$$

I_c is the intensity of the coherent scattered light and I_{inc} is that of the incoherent scattered light. ψ is the phase difference between the diffracted light and the coherent scattered light. The output signal $V(t)$ described in eq 6 contains the homodyne and the heterodyne contributions; the first term in the right-hand side and the second term, relatively. Köhler and his co-workers separate the heterodyne signals by the phase stabilization technique.[21] This heterodyne detection is regarded as the advantageous choice in terms of the statistical noise and the robustness against systematic errors.[21] We, however, adopted homodyne detection and analyzed the output signal $V(t)$ using the following equations. By the direct detection, measurements can be performed by a rather simple measuring system.

Substituting eq 5 into eq 6, the output for the mass diffusion part (Figure 1d) is described as[29]

$$V(t) - V(\infty) = A\exp(-2t/\tau_D) + D\exp(-t/\tau_D) \quad (7)$$

A is the amplitude factor for the diffracted light and D is that for the coherent scattered light. $V(\infty)$ is the output voltage, which is proportional to the total scattered light. Similarly, substituting eq 3 into eq 6, the output for the Soret effect part (Figure 1b) is described as

$$V(t) - V(\infty) = A'\left[\{1-\zeta(t)\}^2 + \frac{1}{A/D}\zeta(t_h)\{1-\zeta(t)\}\right] \quad (8)$$

with

$$\zeta(t) = S_T c_0(1-c_0)(\partial n/\partial c)\cdot(\partial n/\partial T)^{-1}\{1-\exp(-t/\tau_D)\} \quad (9)$$

in which t_h is the heating time and A' is the factor of proportionality. Using the values of τ_D, A, D, and $V(\infty)$ calculated from the decay signal by mass diffusion, the number of variables for the analysis can be decreased. In the curve-fitting analysis, the optimum values of A' and the parameter Γ which is the coefficient of $\{1-\exp(-t/\tau_D)\}$ in the right-hand of eq 9 are searched.

$$\Gamma = S_T c_0(1-c_0)(\partial n/\partial c)\cdot(\partial n/\partial T)^{-1} \quad (10)$$

Because $\partial n/\partial T$ and $\partial n/\partial c$ can be evaluated by a refractometer, the Soret coefficient is calculated.

$$S_T = \frac{\Gamma(\partial n/\partial T)}{c_0(1-c_0)(\partial n/\partial c)} \quad (11)$$

We are thus able to derive S_T and D_{12} simultaneously.

EXPERIMENTAL APPARATUS

Figure 2 is a schematic illustration of the experimental apparatus. As a heating laser, we use a CW solid-state laser

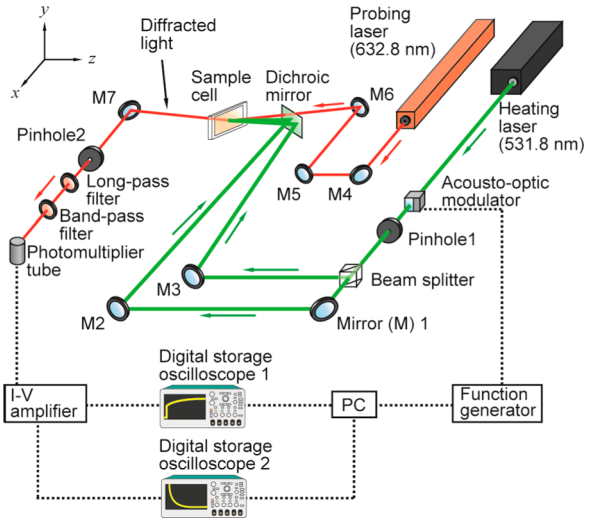

Figure 2. Experimental apparatus for measuring the Soret coefficient and the diffusion coefficient with the wavelengths of 531.8 nm (the heating laser) and 632.8 nm (the probing laser).

(Verdi G5 SLM, Coherent) with the wavelength of 531.8 nm, the maximum power of 5 W, and the beam waists of 2.39 mm (horizontal) and 2.17 mm (horizontal). Because this laser has a very narrow line width (within 5 MHz), it is easy to form an almost ideal interference pattern with high visibility. Since the signal during the heating is used for the analysis for the measurement of the Soret coefficient, the heating laser must be shuttered in pulse corresponding with the theory. We therefore chose an acousto-optic modulator (AOM; M1133-aQ80L-2, Isomet) for shuttering the continuous light of the heating laser in pulse. The rise time of this AOM is fast enough (114 ns per mm beam waist) for millisecond-order shuttering. The interaction material is quartz, which scarcely absorbs the light of 531.8 nm (transmission > 99.5 %), and thus the effect of the thermal lens by the heating laser on the measurement can be ignored. The AOM is controlled by a function synthesizer (WF1956, NF Corp.). The heating laser is split into two beams of the same intensity with a nonpolarized beam splitter (NPCH-20-5320, Sigma Koki). The two beams are adjusted to cross at the sample with the crossing angle of θ. Before the incidence to the sample, the heating laser is reflected by a dichroic mirror (SDM570S, Sigma Koki), which reflects the heating laser but transmits the probing laser.

As a probing laser, we use a He−Ne laser (GLG5730, NEC Corp.) with the wavelength of 632.8 nm, 25 mW power, and the beam waist of 1.2 mm. This laser is adjusted to enter the interference area of the sample at the Bragg angle. The deflected probing beam is detected by a photomultiplier tube (R9110, Hamamatsu Photonics) in the homodyne scheme. Because the absolute value of the signal during heating is important for the measurement of the Soret coefficient, the detection of the light by the heating laser or other disturbing lights must be prohibited. We therefore use a long-pass filter (YIF-BA575IFS, Sigma Koki) and a band-pass filter (FF02-632/22-25, Semrock), as well as a pinhole, for more secure blocking of the light from the heating laser. The long-pass filter

DOI: 10.1021/acs.jced.5b00609
J. Chem. Eng. Data 2015, 60, 3621−3630

cuts the light of the wavelengths shorter than 546 nm, and the transmission at the wavelength of the heating laser is < 0.1 %. The band-pass filter cuts the wavelengths except for 621 nm to 643 nm, and the transmission at the wavelength of the heating laser is < 10^{-5} %.

The output signal from the photomultiplier tube is amplified by a variable gain current−voltage amplifier (DLPCA-200, Femto) and is sent to digital oscilloscopes. We synchronously use two oscilloscopes (DPO3014 and TDS3032B, Tektronix) in order to display and record the generation signal of the concentration distribution and its decay signal independently. The signals are transferred to a desktop computer for the data analysis. The control of the instruments such as the function synthesizer and the data analysis are performed by the LabVIEW software program (National Instruments).

We used two types of sample cell. The first has a screw cap and is used for mixtures of high-volatility organic solvents, and the thickness for the sample is 500 μm. The second type of sample cell consists of two quartz glass plates; one side of one plate is etched at a depth of 200 μm. This cell is suitable for deep-colored mixtures. After the sample is enclosed in the cell, the sample cell is mounted on a copper block cell holder.[29] Water from a thermostat bath (NCB-3100, Tokyo Rikakikai) flows in this sample holder to control the temperature of the sample. The temperature control accuracy of this bath is ± 0.03 K. For the monitoring of the temperature, a thin flexible platinum resistance thermometer (NFR-CF2-0505-30-100S-1-2000TF-A-4-M4Y, Netsushin) with the tolerance of ± (0.15 + 0.002|T − 273.15|) K is mounted on the sample holder. The resistance value is measured by a digital multimeter (7461A, ADC Corp.), and the data are transferred to the desktop computer, which calculates the temperature value with the LabVIEW program.

EXPERIMENTAL PROCEDURE

Materials. The mixture of toluene/*n*-hexane consisted of toluene (99.5 %, Wako) and *n*-hexane (> 96 %, Wako). The binary benchmark mixtures were composed of three types of hydrocarbons: *n*-dodecane ($C_{12}H_{26}$, 99 %), isobutylbenzene (IBB, 99.5 %), and 1,2,3,4-tetrahydronaphthalene (THN, > 98 %), all from Acros Organics. These chemicals were used without further purification. The components were weighed by an electronic balance (EB-330H, Shimadzu) with the readability of 0.001 g, and (5 to 10) g mixtures were prepared. For absorption of the heating laser, a small amount of dye (quinizarin) was added. We have checked experimentally that the appropriate addition of dye does not affect the measurement.[29] For the OPV cast solution systems, we chose the commonly used organic n-type semiconductors [6,6]-phenyl-C61-butyric acid methyl ester (PCBM; 99 %, Solenne), and [60]Fullerene (99.5 %, MTR), and the organic solvent *o*-dichlorobenzene (ODCB; 98 %, Wako) without further purification. These samples were weighed by an electronic analytical balance (XS205, Mettler Toledo) with the readability of 0.01 mg in a nitrogen-purged glove box in which the oxygen concentration was within 0.1 %, and the humidity was within 0.1 %. All of the samples were sufficiently ultrasonicated before the cell was filled.

Measurement of Contrast Factor. To calculate the Soret coefficient with eq 11, the contrast factors $\partial n/\partial T$ and $\partial n/\partial c$ must be evaluated in advance. An Abbe refractometer (DR-A1, Atago) with the minimum scale of 0.0001 was used for the measurement of contrast factors. The wavelength of the light source in this refractometer is 589 nm. Using the refractometer, we measured the refractive index of the sample with different temperatures and concentrations. The refractive indices were measured under the atmospheric pressure of 101 kPa. The data were plotted on a refractive index graph against the temperature and a refractive index graph against the concentration, and contrast factors were determined from the slope of the regression curve.

Optical Alignment and Data Evaluation. The two beams of the heating laser are adjusted to cross at the sample. The fringe spacing Λ is expressed by

$$\Lambda = \frac{\lambda_h}{2 \sin(\theta/2)} \tag{12}$$

where θ is the crossing angle of the heating laser beams and λ_h is the wavelength of the heating laser. Usually the fringe spacing Λ is adjusted to 5 μm. The interference pattern is observed by a laser beam profiler (NanoScan, Ophir) with the sampling resolution of 11.4 nm. In the measurement, usually eight signals were averaged and then analyzed by the LabVIEW program based on the Levenberg−Marquardt method. All the measurements were performed under the atmospheric pressure of 101 kPa.

In the data evaluation process by the nonlinear least-squares method, first, the parameters τ_D, A, D, and $V(\infty)$ in eq 7 are calculated from the mass diffusion part of the signal (Figure 1d). We assess the reliability of the data by the value of A/D. When the value of D is much larger than the value of A, we regard the data as less reliable due to the relatively large effect of the undesirable scattered light. We thus pick out the data with $A/D \geq 10$ empirically.[29] Substituting the calculated value of τ_D and Λ measured by the beam profiler into eq 4, the diffusion coefficient D_{12} is derived. After the evaluation of the mass diffusion part of the signal, the Soret effect part (Figure 1b) is analyzed with eqs 8 and 9. The fitting parameters are Γ and A', because the values of τ_D, A, D, and $V(\infty)$ are already derived. Substituting the calculated value of Γ, $\partial n/\partial T$, and $\partial n/\partial c$ measured by the refractometer and c_0 into eq 11, the Soret coefficient S_T is calculated. The thermodiffusion coefficient D_T is calculated as the product of D_{12} and S_T.

RESULT AND DISCUSSION

Toluene/*n*-Hexane (Evaluation of Uncertainties). Concerning the mixture of toluene/*n*-hexane, the contrast factors used for the analysis are listed in Table 1. Although the wavelength of the light source of our refractometer is 589 nm, the differences between the measured contrast factors and that measured by 633 nm (Köhler et al.[23]) are insignificant. The experimental results obtained for the diffusion coefficient, the thermodiffusion coefficient, and the Soret coefficient of toluene/*n*-hexane are presented in Table 2. Here, we describe the evaluation of the uncertainties of the diffusion coefficient and Soret coefficient. The diffusion coefficient D_{12} is represented by the fringe spacing Λ and the decay time constant of concentration τ_D as described in eq 4. Then the combined standard uncertainty of diffusion coefficient $u_c(D_{12})$ is expressed by

$$u_c(D_{12}) = \sqrt{\left(\frac{\partial f_D}{\partial \tau_D}\right)^2 u^2(\tau_D) + \left(\frac{\partial f_D}{\partial \Lambda}\right)^2 u^2(\Lambda)} \tag{13}$$

where $f_D = (1/\tau_D)\cdot\{\Lambda/(2\pi)\}^2$ is the functional relationship between the measured D_{12} and the input quantities. Although the uncertainties of temperature $u(T)$ and concentration $u(c)$ affect $u_c(D_{12})$, they are not included in eq 13 because $u(T)$ and $u(c)$ are so small that the effect on $u_c(D_{12})$ is within 0.1 %.The uncertainty of the decay time constant of concentration $u(\tau_D)$

DOI: 10.1021/acs.jced.5b00609
J. Chem. Eng. Data 2015, 60, 3621−3630

Table 1. Contrast Factors of Toluene/*n*-Hexane at T = 298.2 K[a]

$c_{toluene}$	$\partial n/\partial c$	$\frac{u(\partial n/\partial c)}{\lvert\partial n/\partial c\rvert}\cdot 100$	$\partial n/\partial T/10^{-4}\,K^{-1}$	$\frac{u(\partial n/\partial T)}{\lvert\partial n/\partial T\rvert}\cdot 100$
0.263 ($x_{toluene}$ = 0.250)[b]	0.1094	1.6	−5.08	3.7
0.517 ($x_{toluene}$ = 0.500)	0.1204	1.4	−5.69	3.7
0.762 ($x_{toluene}$ = 0.750)	0.1314	1.9	−6.12	5.5

[a]Standard uncertainties u are $u(T)$ = 0.1 K and $u(c)$ = 0.0001. [b]$x_{toluene}$ is the mole fraction of toluene.

Table 2. Concentration Dependence of the Diffusion Coefficient and the Soret Coefficient of Toluene/*n*-Hexane at T = 298.2 K[a]

$c_{toluene}$	$D_{12}/10^{-9}\,m^2\,s^{-1}$	$\frac{u(D_{12})}{\lvert D_{12}\rvert}\cdot 100$	$S_T/10^{-3}\,K^{-1}$	$\frac{u(S_T)}{\lvert S_T\rvert}\cdot 100$
0.263 ($x_{toluene}$ = 0.250)	3.68	2.6	3.79	3.9
0.517 ($x_{toluene}$ = 0.500)	2.78	0.5	4.98	4.1
0.762 ($x_{toluene}$ = 0.750)	2.47	0.7	5.79	5.9

[a]Standard uncertainties u are $u(T)$ = 0.1 K and $u(c)$ = 0.0001.

was estimated by the variance of the 10-times measurement of τ_D at the same interference fringe Λ. The uncertainty of fringe spacing $u(\Lambda)$ was estimated by the resolution of the beam profiler and the variance of the five-times measurement of Λ at the same condition. The relative expanded combined standard uncertainties of D_{12} with the coverage factor of k = 2 for toluene/*n*-hexane were estimated to be (0.9 to 5.2) % depending on the concentration, by taking into account the $u(\tau_D)$ of (0.2 to 2.6) % and $u(\Lambda)$ of 0.2 %. Considering the uncertainties of Γ, $\partial n/\partial c$, and $\partial n/\partial T$, the combined standard uncertainty of the Soret coefficient $u_c(S_T)$ is expressed by

$$u_c(S_T) = \left(\left(\frac{\partial f_s}{\partial \Gamma}\right)^2 u^2(\Gamma) + \left\{\frac{\partial f_s}{\partial(\partial n/\partial c)}\right\}^2 u^2(\partial n/\partial c) + \left\{\frac{\partial f_s}{\partial(\partial n/\partial T)}\right\}^2 u^2(\partial n/\partial T)\right)^{1/2} \quad (14)$$

where f_s is the functional relationship between the measured S_T and the input quantities. The uncertainty of the decay time constant of concentration $u(\tau_D)$ is not involved in eq 14 because the effect on $u_c(S_T)$ is small enough, as are those of $u(T)$ and $u(c)$. The uncertainty $u(\Gamma)$ was estimated by the 10-times measurement of Γ at the same interference fringe Λ. The uncertainties of $u(\partial n/\partial c)$ and $u(\partial n/\partial T)$ were estimated by the analysis of the variances of regression coefficients in the regression curve of the refractive index against the concentration or the temperature. The relative expanded combined standard uncertainties of S_T (k = 2) for toluene/*n*-hexane were estimated as (7.9 to 12) % depending on the concentration, by taking into account $u(\Gamma)$ of (0.3 to 0.9) %, $u(\partial n/\partial c)$ of (0.8 to 1.9) %, and $u(\partial n/\partial T)$ of (3.7 to 5.5) %. Figures 3 and 4 show the experimental results for the diffusion coefficient and Soret coefficient on toluene/*n*-hexane. Our experimental data were smoothed by the quadratic polynomials described in eqs 15 or 16, because there is no recommended correlation for the concentration dependence of D_{12} or S_T.

$$D_{12}/(m^2\,s^{-1}) = \sum_{i=0}^{2} a_i x_{toluene}{}^i \quad (15)$$

$$S_T/(K^{-1}) = \sum_{i=0}^{2} b_i x_{toluene}{}^i \quad (16)$$

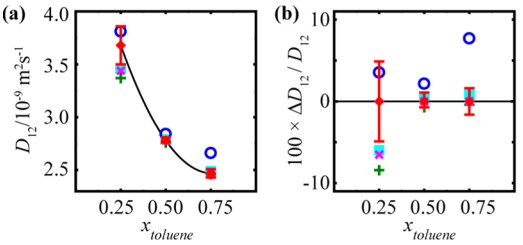

Figure 3. (a) Diffusion coefficient D_{12} of toluene/*n*-hexane against the mole fraction of toluene $x_{toluene}$. (b) Relative differences $\Delta D_{12}/D_{12} = \{D_{12}(expt) - D_{12}(calc)\}/D_{12}(calc)$ of the experimental diffusion coefficients $D_{12}(expt)$ from those calculated with eq 15 $D_{12}(calc)$: red ◆, present study at T = 298.2 K; blue ○, ref 29 at T = 298.15 K; blue ■, ref 23 at T = 296 K; +, ref 31 at T = 298 K; red ×, ref 17 at T = 298 K. The solid line is the fitting curve obtained using eq 15. Error bars are the standard deviation (SD) of the measurements.

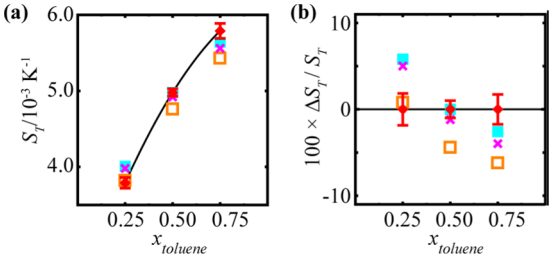

Figure 4. (a) Soret coefficient S_T of toluene/*n*-hexane against the mole fraction of toluene $x_{toluene}$. (b) Relative differences $\Delta S_T/S_T = \{S_T(expt) - S_T(calc)\}/S_T(calc)$ of the experimental Soret coefficients $S_T(expt)$ from those calculated with eq 16 $S_T(calc)$: red ◆, the present study at T = 298.2 K; blue ■, ref 23 at T = 296 K; red ×, ref 17 at T = 298 K; red □, ref 32 at T = 298 K. The solid line is the fitting curve obtained by using eq 16. Error bars: SD of the measurements.

Table 3. Values of Coefficients a_i and b_i in eqs 15 and 16

i	a_i	b_i
0	$5.17\cdot10^{-9}$	$2.22\cdot10^{-3}$
1	$-7.14\cdot10^{-9}$	$7.04\cdot10^{-3}$
2	$4.72\cdot10^{-9}$	$-3.04\cdot10^{-3}$

The values of coefficients a_i and b_i are listed in Table 3. There is good agreement between our results and those reported by other groups within the range of uncertainties.

DOI: 10.1021/acs.jced.5b00609
J. Chem. Eng. Data 2015, 60, 3621−3630

Table 4. Contrast Factors of the Binary Benchmark Mixtures at T = 298.2 K[a]

sample	c	$\partial n/\partial c$	$\frac{u(\partial n/\partial c)}{\lvert\partial n/\partial c\rvert}\cdot 100$	$\partial n/\partial T$ /10^{-4} K^{-1}	$\frac{u(\partial n/\partial T)}{\lvert\partial n/\partial T\rvert}\cdot 100$
IBB/$C_{12}H_{26}$	0.500	0.0634	1.2	−4.78	4.3
THN/$C_{12}H_{26}$	0.500	0.1180	1.4	−4.75	2.4
THN/IBB	0.500	0.0548	0.8	−4.87	7.8

[a]Standard uncertainties u are $u(T)$ = 0.1 K and $u(c)$ = 0.0001.

Table 5. Diffusion Coefficients and Soret Coefficients of the Binary Benchmark Mixtures at T = 298.2 K[a]

sample	c	$D_{12}/10^{-10}$ m^2 s^{-1}	$\frac{u(D_{12})}{\lvert D_{12}\rvert}\cdot 100$	S_T /10^{-3} K^{-1}	$\frac{u(S_T)}{\lvert S_T\rvert}\cdot 100$
IBB/$C_{12}H_{26}$	0.500	9.63	2.7	4.10	4.9
THN/$C_{12}H_{26}$	0.500	6.63	1.6	10.2	7.9
THN/IBB	0.500	8.71	4.5	3.59	6.0

[a]Standard uncertainties u are $u(T)$ = 0.1 K and $u(c)$ = 0.0001.

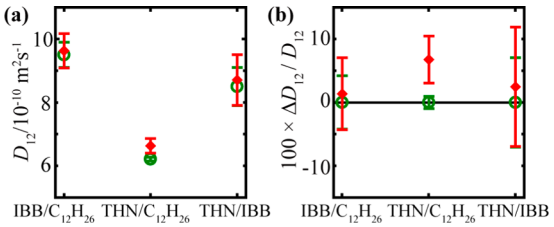

Figure 5. (a) Diffusion coefficient D_{12} of the binary benchmark mixtures (c = 0.500). (b) Relative differences $\Delta D_{12}/D_{12}$ = {D_{12}(expt) − D_{12}(benchm)}/D_{12}(benchm) of the experimental Soret coefficients in the present study D_{12}(expt) from those in ref 33 D_{12}(benchm): red ◆, the present study at T = 298.2 K; green ○, benchmark values in ref 33 at T = 298 K. Error bars: SD.

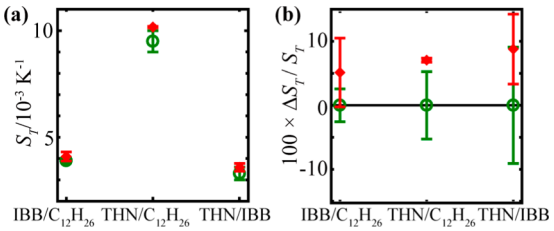

Figure 6. (a) Soret coefficient S_T of the binary benchmark mixtures (c = 0.500). (b) Relative differences $\Delta S_T/S_T$ = {S_T(expt) − S_T(benchm)}/S_T(benchm) of the experimental Soret coefficients in the present study S_T(expt) from those in ref 33 S_T(benchm): red ◆, the present study at T = 298.2 K; green ○, benchmark values in ref 33 at T = 298 K. Error bars: SD.

Binary Benchmark Mixtures. The so-called Fontainebleau benchmark values for the measurement of the Soret coefficient were proposed by Platten et al.[33] for the three binary mixtures composed of *n*-dodecane, isobutylbenzene, and 1,2,3,4-tetrahydronaphthalene with the mass fraction of c = 0.500 at T = 298 K as the average value of five groups, using four different techniques.[33] We carried out measurements on the benchmark mixtures in order to compare our results and the benchmark values. The contrast factors that we used for the analysis are given in Table 4. The experimental results obtained for the diffusion coefficient and Soret coefficient on the binary benchmark mixtures are presented in Table 5. Our experimental results for the diffusion coefficient and Soret coefficient are shown in Figures 5 and 6. In the deviation plots, it is shown that our experimental results of the diffusion coefficient and the Soret coefficient agree with the benchmark values within ± 10 %. The relative expanded uncertainty of D_{12} and S_T (k = 2) for the benchmark mixtures have been estimated as (3.3 to 9.1) % and (10 to 16) % depending on the sample, respectively. Therefore, the validity of the constructed apparatus for SFRS was confirmed.

OPV Cast Solution System. The measured refractive index values of [60]fullerene/ODCB and PCBM/ODCB for evaluating the contrast factors are listed in Table 6. In the measurement of refractive index values, it was difficult to obtain an adequate reading of the values for denser solution, and the measured values showed larger scattering. Because we have not acquired all of the refractive index values for the ranges of concentrations and temperatures needed for the data analysis, we used the fixed contrast factors listed in Table 7 in the analysis of the samples for the entire range of temperature or concentration. Obviously, the contrast factors highly affect the calculation of the Soret coefficient, and their precise evaluation is crucial. However, we consider that the errors introduced by using the fixed contrast factors are included in the range of the uncertainties of them, because of the small difference of measured concentration due to the low solubilities[40,41] and the assumption of a linear relationship between the refractive index

Table 6. Temperature and Concentration Dependence of the Refractive Index n for PCBM/ODCB and [60]Fullerene/ODCB at p = 101 kPa Measured by Abbe Refractometer[a]

	T/K				
$10^3 \cdot c$	288.2	298.2	308.2	318.2	328.2
	[60]fullerene/ODCB				
0	1.5523	1.5489	1.5438	1.5386	1.5332
3.84	1.5549	1.5502	1.5457	1.5408	1.5354
7.69	1.5577	1.5522	1.5478	1.5425	1.5395
11.5	1.5598	1.5538	1.5497	1.5456	
15.4	1.5624				
	PCBM/ODCB				
1.92	1.5532	1.5488	1.5432	1.5385	1.5334
3.84	1.5529	1.5494	1.5441	1.5386	1.5334
5.77	1.5542	1.5494	1.5447	1.5391	1.5342
7.69	1.5547	1.5500	1.5453	1.5400	1.5348

[a]Standard uncertainties u are $u(T)$ = 0.1 K, $u(c)$ = 0.000001, $u(p)$ = 2 kPa, and $u(n)$ = 0.0005.

DOI: 10.1021/acs.jced.5b00609
J. Chem. Eng. Data 2015, 60, 3621−3630

Table 7. Contrast Factors Used for the Analysis of [60]Fullerene/ODCB and PCBM/ODCB[a]

sample	$\partial n/\partial c$	$\frac{u(\partial n/\partial c)}{\lvert\partial n/\partial c\rvert}\cdot 100$	$\partial n/\partial T/10^{-4}\mathrm{K}^{-1}$	$\frac{u(\partial n/\partial T)}{\lvert\partial n/\partial T\rvert}\cdot 100$
[60]fullerene/ODCB	0.438 (T = 298.2 K)	6.4	−4.61 (c = 7.69·10^{-3})	5.2
PCBM/ODCB	0.312 (T = 298.2 K)	24	−5.03 (c = 3.84·10^{-3})	1.7

[a]Standard uncertainties u are $u(T)$ = 0.1 K and $u(c)$ = 0.000001.

Table 8. Temperature Dependence of the Diffusion Coefficient D_{12}, Thermodiffusion Coefficient D_T, and Soret Coefficient S_T for PCBM/ODCB of c = 7.69·10^{-3} (10 mg·mL^{-1}) and [60]fullerene/ODCB of c = 7.69·10^{-3} (10 mg·mL^{-1})[a]

T/K	$D_{12}/10^{-10}$ m^2 s^{-1}	$u(D_{12})/\lvert D_{12}\rvert\cdot 100$	$D_T/10^{-11}$ m^2 s^{-1} K^{-1}	$u(D_T)/\lvert D_T\rvert\cdot 100$	$S_T/10^{-2}$ K^{-1}	$u(S_T)/\lvert S_T\rvert\cdot 100$
[60]fullerene/ODCB						
288.2	3.78	0.6	0.723	8.4	1.91	8.3
293.2	4.39	1.3	0.798	8.5	1.82	8.4
298.2	4.60	1.1	1.17	8.4	2.54	8.3
303.2	5.19	1.9	0.931	8.5	1.79	8.3
308.2	6.13	1.3	1.34	8.4	2.18	8.3
313.2	6.55	1.1	1.69	8.3	2.58	8.3
318.2	7.34	1.5	1.58	8.4	2.15	8.3
323.2	7.46	2.8	1.69	9.1	2.26	8.6
328.2	8.22	0.8	2.17	8.3	2.63	8.2
333.2	8.52	1.0	2.17	8.3	2.55	8.3
PCBM/ODCB						
288.2	2.79	0.6	0.814	25	2.92	25
293.2	3.07	0.6	0.901	25	2.93	25
298.2	3.31	0.7	0.957	25	2.89	25
303.2	3.58	1.1	1.08	25	3.03	25
308.2	4.07	1.3	1.14	25	2.80	25
313.2	4.21	1.2	1.10	25	2.61	25
318.2	4.60	1.7	1.19	25	2.58	25
323.2	4.85	1.4	1.31	25	2.71	25
328.2	5.00	1.2	1.32	25	2.63	25
333.2	5.53	1.0	1.23	25	2.23	25

[a]Standard uncertainties u are $u(T)$ = 0.1 K and $u(c)$ = 0.000001.

and the concentration and temperature, as observed in the hydrocarbon mixtures.[42]

The temperature dependence of the diffusion coefficient, the thermodiffusion coefficient and the Soret coefficient in [60]fullerene/ODCB and PCBM/ODCB are presented in Table 8. The measured diffusion coefficient D_{12} against temperature T is shown in Figure 7a, along with the theoretical calculation using the Stokes−Einstein (SE) equation.[43] In the SE equation, the diffusion coefficient D_{12} is expressed by the temperature T, the hydrodynamic radius of solute R, and the viscosity of solvent η.

$$D_{12} = \frac{k_B T}{f_T \pi \eta R} \tag{17}$$

where k_B is the Boltzmann constant and f_T is the boundary condition parameter, which is f_T = 4 for the "slip" condition and f_T = 6 for the "stick" condition. Substituting the viscosity of o-dichlorobenzene η as a function of temperature calculated by the experimental data[44] and the radius of [60]fullerene R calculated by the partial molar volume[45] into eq 17, we found that the experimental data on [60]fullerene/ODCB sufficiently agree with the calculation using the SE equation with f_T = 4 of the slip condition, as shown in the deviation plot of Figure 8.

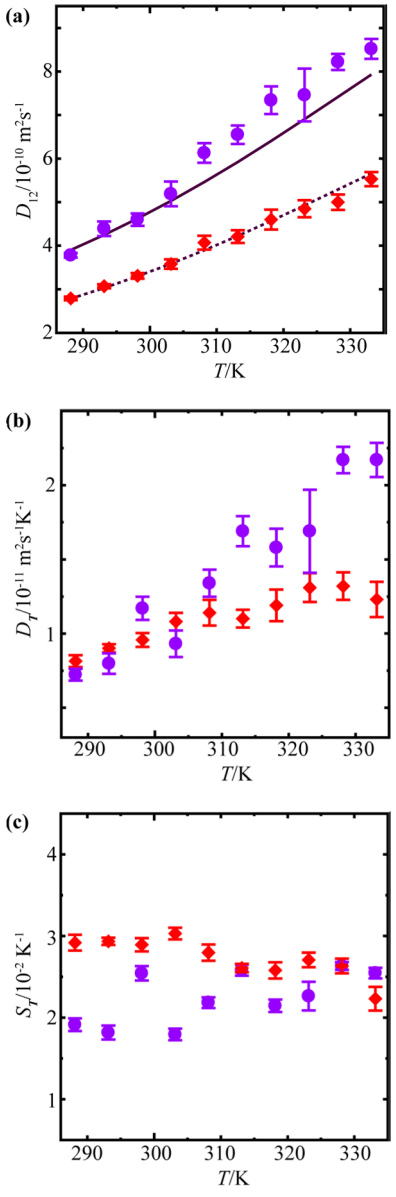

Figure 7. Temperature dependence of (a) diffusion coefficient D_{12}, (b) thermodiffusion coefficient D_T, and (c) Soret coefficient S_T: purple ●, [60]fullerene/ODCB (10 mg·mL^{-1}); red ◆, PCBM/ODCB (10 mg·mL^{-1}). Solid line: calculated by the Stokes−Einstein (SE) eq (eq 17) with the Stokes radius of 1.07 nm. Dashed line: calculated by the SE eq (eq 17) with the Stokes radius of 1.50 nm. Error bars: SD of the measurements.

The fitting was then conducted with f_T = 4 for the experimental data on PCBM/ODCB, and there was good agreement between the data and calculation with the radius of PCBM R = 1.50 nm. Considering the structure of PCBM, this value seems to be reasonable. The dependency of the thermodiffusion coefficient and Soret coefficient on the temperature are

DOI: 10.1021/acs.jced.5b00609
J. Chem. Eng. Data 2015, 60, 3621−3630

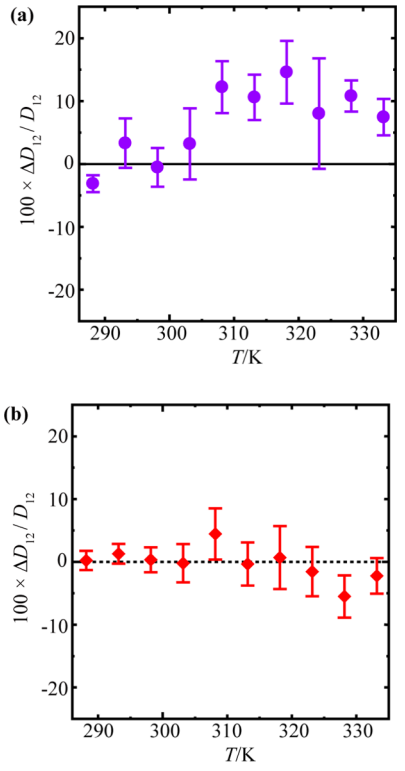

Figure 8. Relative differences $\Delta D_{12}/D_{12} = \{D_{12}(\text{expt}) - D_{12}(\text{calc})\}/D_{12}(\text{calc})$ of the experimental diffusion coefficients D_{12}(expt) from those calculated with the SE eq (eq 17) D_{12}(calc). (a) Purple ●, [60]fullerene/ODCB (10 mg·mL^{-1}). Solid line: SE equation with the Stokes radius of 1.07 nm. (b) Red ◆, PCBM/ODCB (10 mg·mL^{-1}). Dashed line: SE equation with the Stokes radius of 1.50 nm. Error bars: SD of the measurements.

demonstrated in Figure 7b,c. Compared to the experimental result of the thermodiffusion coefficient on [60]fullerene/toluene,[46] our result is considered to be derived in a reasonable order. The temperature dependence of the Soret coefficient seems to be small, despite the apparent temperature dependency of the diffusion coefficient. Although the experimental works on the temperature dependence of the S_T are limited, the rather apparent changes of S_T with the temperature have been reported on liquid mixtures such as toluene/*n*-hexane,[17] water/ethanol,[47] and dibromohexane/cyclohexane,[48] depending on

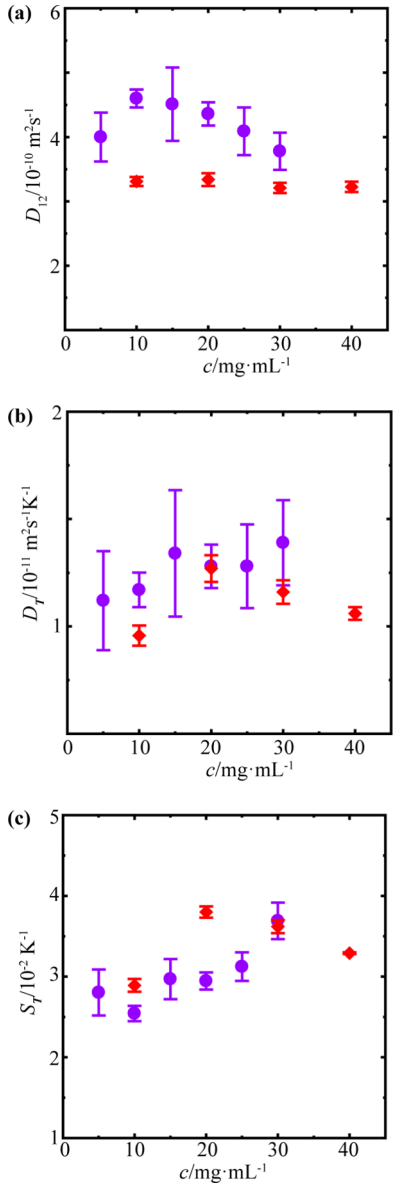

Figure 9. Concentration dependence of (a) diffusion coefficient D_{12}, (b) thermodiffusion coefficient D_T, and (c) Soret coefficient S_T: purple ●, [60]fullerene/ODCB at T = 298.2 K; red ◆, PCBM/ODCB at T = 298.2 K. Error bars: SD of the measurements.

Table 9. Concentration Dependence the Diffusion Coefficient D_{12}, Thermodiffusion Coefficient D_T and Soret Coefficient S_T for PCBM/ODCB (T = 298.2 K) and [60]Fullerene/ODCB (T = 298.2 K)[a]

$10^3 \cdot c$	$D_{12}/10^{-10}$ m^2 s^{-1}	$u(D_{12})/\lvert D_{12}\rvert \cdot 100$	$D_T/10^{-11}$ m^2 s^{-1} K^{-1}	$u(D_T)/\lvert D_T\rvert \cdot 100$	$S_T/10^{-2}$ K^{-1}	$u(S_T)/\lvert S_T\rvert \cdot 100$
			[60]fullerene/ODCB			
3.84 (5 mg·mL^{-1})	4.00	3.3	1.12	9.6	2.80	9.0
7.69 (10 mg·mL^{-1})	4.60	1.1	1.17	8.4	2.54	8.3
11.5 (15 mg·mL^{-1})	4.51	4.6	1.34	9.8	2.97	8.7
15.4 (20 mg·mL^{-1})	4.36	1.4	1.28	8.4	2.95	8.3
19.2 (25 mg·mL^{-1})	4.09	3.2	1.28	9.0	3.12	8.4
23.1 (30 mg·mL^{-1})	3.78	2.7	1.39	8.9	3.69	8.5
			PCBM/ODCB			
7.69 (10 mg·mL^{-1})	3.31	0.7	0.957	25	2.89	25
15.4 (20 mg·mL^{-1})	3.34	1.0	1.27	25	3.80	25
23.1 (30 mg·mL^{-1})	3.21	0.9	1.16	25	3.62	25
30.7 (40 mg·mL^{-1})	3.23	0.9	1.06	25	3.29	25

[a]Standard uncertainties u are $u(T)$ = 0.1 K and $u(c)$ = 0.000001.

DOI: 10.1021/acs.jced.5b00609
J. Chem. Eng. Data 2015, 60, 3621−3630

the concentration. The tendency similar to the present work, however, can be found in the experimental results on the solution of polysaccharide (pullulan in dimethyl sulfoxide),[49] in terms of not only the small dependency of S_T on the temperature but also the linear increase of D_T with the temperature. The concentration dependence of the diffusion coefficient, the thermodiffusion coefficient, and the Soret coefficient in [60]fullerene/ODCB and PCBM/ODCB is illustrated in Table 9. As shown in Figure 9, the dependency of the diffusion coefficient on the concentration is not so large, but a reduction of the diffusion coefficient for denser concentrations was observed. We speculate that this trend was caused by the aggregation of [60]fullerene or PCBM. For [60]fullerene/ODCB, the Soret coefficient rises with the concentration. On the other hand, the opposite trend was observed for PCBM/ODCB. As described above, we measured the diffusion coefficient and Soret coefficient in wide ranges of temperature and concentration and detected a difference in trends between [60]fullerene/ODCB and PCBM/ODCB.

CONCLUSION

Our experimental apparatus and data evaluation method based on the Soret forced Rayleigh scattering (SFRS) method for the simultaneous measurement of the Soret coefficient and the diffusion coefficient in binary mixtures were presented. The validation was confirmed by the measurements of toluene/*n*-hexane and the binary benchmark mixtures. The estimated uncertainties of the diffusion coefficient with a 0.95 level of confidence ($k = 2$) are within 5.2 % for toluene/*n*-hexane and within 9.1 % for the benchmark mixtures. As for the uncertainties of the Soret coefficient, we estimated that it is within 12 % for toluene/*n*-hexane and within 16 % for the benchmark mixtures. Using the experimental apparatus, measurements were obtained on the cast solution systems of OPV ([60]fullerene/ODCB and PCBM/ODCB). We also evaluated the different trends of mass transport between [60]fullerene/ODCB and PCBM/ODCB, although the results involve relatively large uncertainties due to the difficulty in the measurement of contrast factors.

AUTHOR INFORMATION

Corresponding Author

*Tel./Fax: +81-45-566-1735. E-mail: nagasaka@sd.keio.ac.jp.

Funding

The work described in this paper was carried out under a Grant-in Aid for Scientific Research (S) (No. 24226006) from the Japan Society for the Promotion of Science (JSPS).

Notes

The authors declare no competing financial interest.

REFERENCES

(1) Li, G.; Shrotriya, V.; Huang, J.; Yao, Y.; Moriarty, T.; Emery, K.; Yang, Y. High-efficiency solution processable polymer photovoltaic cells by self-organization of polymer blends. *Nat. Mater.* **2005**, *4*, 864−868.

(2) Thompson, B. C.; Fréchet, J. M. J. Polymer−fullerene composite solar cells. *Angew. Chem., Int. Ed.* **2008**, *47*, 58−77.

(3) You, J.; Dou, L.; Yoshimura, K.; Kato, T.; Ohya, K.; Moriarty, T.; Emery, K.; Chen, C. C.; Gao, J.; Li, G.; Yang, Y. A polymer tandem solar cell with 10.6% power conversion efficiency. *Nat. Commun.* **2013**, *4*, 1446.

(4) Krebs, F. C. Fabrication and processing of polymer solar cells: A review of printing and coating techniques. *Sol. Energy Mater. Sol. Cells* **2009**, *93*, 394−412.

(5) Søndergaard, R. R.; Hösel, M.; Krebs, F. C. Roll-to-roll fabrication of large area functional organic materials. *J. Polym. Sci., Part B: Polym. Phys.* **2013**, *51*, 16−34.

(6) Yang, X. N.; Loos, J.; Veenstra, S. C.; Verhees, W. J. H.; Wienk, M. M.; Kroon, J. M.; Michels, M. A. J.; Janssen, R. A. J. Nanoscale morphology of high-performance polymer solar cells. *Nano Lett.* **2005**, *5*, 579−583.

(7) Campoy-Quiles, M.; Ferenczi, T.; Agostinelli, T.; Etchegoin, P. G.; Kim, Y.; Anthopoulos, T. D.; Stavrinou, P. N.; Bradley, D. D. C.; Nelson, J. Morphology evolution via self-organization and lateral and vertical diffusion in polymer: fullerene solar cell blends. *Nat. Mater.* **2008**, *7*, 158−164.

(8) Liu, F.; Gu, Y.; Jung, J. W.; Jo, W. H.; Russell, T. P. On the morphology of polymer-based photovoltaics. *J. Polym. Sci., Part B: Polym. Phys.* **2012**, *50*, 1018−1044.

(9) Yu, G.; Gao, J.; Hummelen, J. C.; Wudl, F.; Heeger, A. J. Polymer photovoltaic cells: enhanced efficiencies via a network of internal donor-acceptor heterojunctions. *Science* **1995**, *270*, 1789−1791.

(10) Brabec, C. J.; Gowrisanker, S.; Halls, J. J. M.; Laird, D.; Jia, S.; Williams, S. P. Polymer-fullerene bulk-heterojunction solar cells. *Adv. Mater.* **2010**, *22*, 3839−3856.

(11) Chen, D.; Nakahara, A.; Wei, D.; Nordlund, D.; Russell, T. P. P3HT/PCBM bulk heterojunction organic photovoltaics: Correlating efficiency and morphology. *Nano Lett.* **2011**, *11*, 561−567.

(12) Zhang, Y.; Diao, Y.; Lee, H.; Mirabito, T. J.; Johnson, R. W.; Puodziukynaite, E.; John, J.; Carter, K. R.; Emrick, T.; Mannsfeld, S. C. B.; Briseno, A. L. Intrinsic and extrinsic parameters for controlling the growth of organic single-crystalline nanopillars in photovoltaics. *Nano Lett.* **2014**, *14*, 5547−5554.

(13) Treat, N. D.; Brady, M. A.; Smith, G.; Toney, M. F.; Kramer, E. J.; Hawker, C. J.; Chabinyc, M. L. Interdiffusion of PCBM and P3HT reveals miscibility in a photovoltaically active blend. *Adv. Energy Mater.* **2011**, *1*, 82−89.

(14) Treat, N. D.; Mates, T. E.; Hawker, C. J.; Kramer, E. J.; Chabinyc, M. L. Temperature dependence of the diffusion coefficient of PCBM in poly(3-hexylthiophene). *Macromolecules* **2013**, *46*, 1002−1007.

(15) Fischer, F.; Hahn, T.; Bässler, H.; Bauer, I.; Strohriegl, P.; Köhler, A. Measuring reduced C60 diffusion in crosslinked polymer films by optical spectroscopy. *Adv. Funct. Mater.* **2014**, *24*, 6172−6177.

(16) Dutrieux, J. F.; Platten, J. K.; Chavepeyer, G.; Bou-Ali, M. M. On the measurement of positive Soret coefficients. *J. Phys. Chem. B* **2002**, *106*, 6104−6114.

(17) Zhang, K. J.; Briggs, M. E.; Gammon, R. W.; Sengers, J. V. Optical measurement of the Soret coefficient and the diffusion coefficient of liquid mixtures. *J. Chem. Phys.* **1996**, *104*, 6881−6892.

(18) Rahman, M. A.; Saghir, M. Z. Thermodiffusion or Soret effect: Historical review. *Int. J. Heat Mass Transfer* **2014**, *73*, 693−705.

(19) Thyagarajan, K.; Lallemand, P. Determination of the thermal diffusion ratio in a binary mixture by forced Rayleigh scattering. *Opt. Commun.* **1978**, *26*, 54−57.

(20) Köhler, W. Thermodiffusion in polymer solutions as observed by forced Rayleigh scattering. *J. Chem. Phys.* **1993**, *98*, 660−668.

(21) Köhler, W.; Rossmanith, P. Aspects of thermal diffusion forced Rayleigh scattering: Heterodyne detection, active phase tracking, and experimental constraints. *J. Phys. Chem.* **1995**, *99*, 5838−5847.

(22) Köhler, W.; Schäfer, R. Polymer analysis by thermal-diffusion forced Rayleigh scattering. *New Developments in Polymer Analytics II; Advances in Polymer Science*; Springer: Berlin, 2000, *151*, 1−59.

(23) Köhler, W.; Müller, B. Soret and mass diffusion coefficients of toluene/n-hexane mixtures. *J. Chem. Phys.* **1995**, *103*, 4367−4370.

(24) Rossmanith, P.; Köhler, W. Polymer polydispersity analysis by thermal diffusion forced Rayleigh scattering. *Macromolecules* **1996**, *29*, 3203−3211.

DOI: 10.1021/acs.jced.5b00609
J. Chem. Eng. Data 2015, 60, 3621−3630

(25) Rauch, J.; Köhler, W. Diffusion and thermal diffusion of semidilute to concentrated solutions of polystyrene in toluene in the vicinity of the glass transition. *Phys. Rev. Lett.* **2002**, *88*, 185901.
(26) Hayashida, K.; Nagasaka, Y. Measurement of mutual diffusion coefficient by the Soret forced Rayleigh scattering method (1st report, examination of the method and measurement of polymer solutions). *Nippon Kikai Gakkai Ronbunshu, B-hen* **1997**, *B63*, 276−281.
(27) Yamamoto, Y.; Nagasaka, Y. Development of the Soret forced Rayleigh scattering method for measurement of mass diffusion coefficient (1st report, development of the measurement system and measurement of the fullerene in solution). *Nippon Kikai Gakkai Ronbunshu, B-hen* **2006**, *B72*, 709−714.
(28) Yamamoto, Y.; Nagasaka, Y. Measurement of mass diffusion coefficient by the Soret forced Rayleigh scattering method (2nd report, theoretical analysis of systematic effect of experimental parameters). *Nippon Kikai Gakkai Ronbunshu, B-hen* **2006**, *B72*, 715−722.
(29) Niwa, M.; Ohta, Y.; Nagasaka, Y. Mass diffusion coefficients of cellulose acetate butyrate in methyl ethyl ketone solutions at temperatures between (293 and 323) K and mass fractions from 0.05 to 0.60 using the Soret forced Rayleigh scattering method. *J. Chem. Eng. Data* **2009**, *54*, 2708−2714.
(30) Nagasaka, Y.; Hatakeyama, T.; Okuda, M.; Nagashima, A. Measurement of the thermal diffusivity of liquids by the forced Rayleigh scattering method: Theory and experiment. *Rev. Sci. Instrum.* **1988**, *59*, 1156−1168.
(31) Ghai, R. K.; Dullien, F. A. L. Diffusivities and viscosities of some binary liquid nonelectrolytes at 25°. *J. Phys. Chem.* **1974**, *78*, 2283−2291.
(32) Bou-Ali, M. M.; Ecenarro, O.; Madariaga, J. A.; Santamaria, C. M.; Valencia, J. J. Thermogravitational measurement of the Soret coefficient of liquid mixtures. *J. Phys.: Condens. Matter* **1998**, *10*, 3321−3331.
(33) Platten, J. K.; Bou-Ali, M. M.; Costesèque, P.; Dutrieux, J. F.; Köhler, W.; Leppla, C.; Wiegand, S.; Wittko, G. Benchmark values for the Soret, thermal diffusion and diffusion coefficients of three binary organic liquid mixtures. *Philos. Mag.* **2003**, *83*, 1965−1971.
(34) Wittko, G.; Köhler, W. Precise determination of the Soret, thermal diffusion and mass diffusion coefficients of binary mixtures of dodecane, isobutylbenzene and 1,2,3,4-tetrahydronaphthalene by a holographic grating technique. *Philos. Mag.* **2003**, *83*, 1973−1987.
(35) Leppla, C.; Wiegand, S. Investigation of the Soret effect in binary liquid mixtures by thermal-diffusion-forced Rayleigh scattering (contribution to the benchmark test). *Philos. Mag.* **2003**, *83*, 1989−1999.
(36) Platten, J. K.; Bou-Ali, M. M.; Dutrieux, J. F. Precise determination of the Soret, thermodiffusion and isothermal diffusion coefficients of binary mixtures of dodecane, isobutylbenzene and 1,2,3,4-tetrahydronaphthalene (contribution of the University of Mons to the benchmark test). *Philos. Mag.* **2003**, *83*, 2001−2010.
(37) Bou-Ali, M. M.; Valencia, J. J. Determination of the thermodiffusion coefficient in three binary organic liquid mixtures by the thermogravitational method (contribution of the Universidad del País Vasco, Bilbao, to the benchmark test). *Philos. Mag.* **2003**, *83*, 2011−2015.
(38) Costesèque, P.; Loubet, J. C. Measuring the Soret coefficient of binary hydrocarbon mixtures in packed thermogravitational columns (contribution of Toulouse University to the benchmark test). *Philos. Mag.* **2003**, *83*, 2017−2022.
(39) Eichler, H. J.; Günter, P.; Pohl, D. W. *Laser-Induced Dynamic Gratings*; Springer: Berlin, Heidelberg, NY, 1986.
(40) Ruoff, R. S.; Tse, D. S.; Malhotra, R.; Lorents, D. Solubility of C60 in a variety of solvents. *J. Phys. Chem.* **1993**, *97*, 3379−3383.
(41) Machui, F.; Langner, S.; Zhu, X.; Abbott, S.; Brabec, C. J. Determination of the P3HT:PCBM solubility parameters via a binary solvent gradient method: Impact of solubility on the photovoltaic performance. *Sol. Energy Mater. Sol. Cells* **2012**, *100*, 138−146.
(42) Yahya, M.; Saghir, M. Z. Prediction and experimental measurement of refractive index in ternary hydrocarbon mixtures. *J. Chem. Eng. Data* **2015**, *60*, 2329−2342.
(43) Cussler, E. L. *Diffusion: Mass Transfer in Fluid Systems*, 3rd ed.; Cambridge Series in Chemical Engineering; Cambridge University Press: New York, 2009.
(44) Griffing, V.; Cargyle, M. A.; Corvese, L.; Eby, D. Temperature coefficients of viscosity of some halogen substituted organic compounds. *J. Phys. Chem.* **1954**, *58*, 1054−1056.
(45) Ruelle, P.; Farina-Cuendet, A.; Kesselring, U. W. Changes of molar volume from solid to liquid and solution: The particular case of C_{60}. *J. Am. Chem. Soc.* **1996**, *118*, 1777−1784.
(46) Martin, A.; Bou-Ali, M. M. Determination of thermal diffusion coefficient of nanofluid: Fullerene−toluene. *C. R. Mec.* **2011**, *339*, 329−334.
(47) Kolodner, P.; Williams, H.; Moe, C. Optical measurement of the Soret coefficient of ethanol/water solutions. *J. Chem. Phys.* **1988**, *88*, 6512−6524.
(48) Wittko, G.; Köhler, W. On the temperature dependence of thermal diffusion of liquid mixtures. *Europhys. Lett.* **2007**, *78*, 46007.
(49) Kishikawa, Y.; Wiegand, S.; Kita, R. Temperature dependence of Soret coefficient in aqueous and nonaqueous solutions of pullulan. *Biomacromolecules* **2010**, *11*, 740−747.

DOI: 10.1021/acs.jced.5b00609
J. Chem. Eng. Data 2015, 60, 3621−3630